Evidence for short-range ferromagnetic order in amorphous $(Gd,Y)_xSi_{1-x}$ alloys

S. Caprara
Dipartimento di Fisica, Università di Roma "La Sapienza," and Istituto Nazionale per la Fisica della Materia, SMC and UdR di Roma 1, Piazzale Aldo Moro 2, 00185 Rome, Italy

N. K. Chumakov, S. Gudenko, and V. Tugushev
RRC Kurchatov Institute, Kurchatov Square 1, 123182 Moscow, Russia

(Received 10 October 2005; revised manuscript received 27 June 2006; published 21 September 2006)

We present electron paramagnetic resonance (EPR) and magnetotransport measurements for amorphous RE_xSi_{1-x} alloys [rare earth (RE) metals are Gd, Y; $0.1<x<0.2$], over a wide range of temperatures and magnetic fields. To explain the experimental results, we use a model in which the structural disorder in the system causes the appearance of regions with a higher electron concentration around nanoscale defects enriched with rare-earth ions (droplets). It is shown that the observed EPR signal can be formed only in the double-bottleneck regime. Then, the temperature dependences for the line position and the linewidth are obtained. We also analyze recent measurements of the temperature- and magnetic-field dependence of the electrical conductivity and Hall effect, and show that the spin polarization of the electron states in the droplets favors a giant negative magnetoresistance and enhances the tendency towards the metal-insulator transition. The ferromagnetic transition temperature and the number of Gd ions inside the nanoscale defect enveloped by the droplet are evaluated from a comparison between the theory and the experimental data. We suggest that amorphous RE_xSi_{1-x} alloys are magnetic materials with unique properties of both strongly inhomogeneous compounds and nanocomposites.

DOI: 10.1103/PhysRevB.74.104204 PACS number(s): 61.43.Dq, 72.20.My, 76.30.Kg

I. INTRODUCTION

The properties of amorphous (*a*-) RE_xSi_{1-x} alloys, with rare-earth (RE) metals RE=Gd,Y and $0.1<x<0.2$, have been actively investigated and discussed in recent years. Various changes occur in the electronic and magnetic structure of these alloys by varying the temperature T and the magnetic induction B, and a giant negative magnetoresistance is observed. The experiments[1–5] indicate that dopant magnetic ions in a heavily disordered semiconductor can combine features of the usual doping-driven metal-insulator transition, typical of amorphous systems, with features of the temperature- and field-driven magnetic transformations.

Indeed, when magnetic Gd ions are doped into the *a*-Si host, the transport properties are severely affected below a characteristic temperature $T^* \approx 10-100$ K (Ref. 6): for $T>T^*$, the electrical conductivity is almost linear with T, like in samples doped with isovalent but nonmagnetic Y, whereas for $T<T^*$, the conductivity is strongly suppressed, as compared to the Y-doped samples, and a giant negative magnetoresistance is found. The low-field magnetization obeys the Curie-Weiss law over a wide range $10\ \mathrm{K}<T<300$ K; at very low T, below the freezing temperature $T_f \sim 5\ \mathrm{K} \ll T^*$, a spin-glass behavior is observed. Samples that are metallic at high T show a tendency towards the metal-insulator transition at low T.

These findings cannot be explained within simple magnetic interaction models. Some years ago, the competition between structural and magnetic disorder in these alloys was analyzed within a model for the Anderson-Mott transition driven by spin disorder.[7,8] The model seems very successful in the low-temperature regime $T \leqslant T_f$, where the spin-glass and the metal-insulator transitions occur. On the other hand, the origin of the features observed in magnetic and transport properties at high temperatures, and the strikingly different behavior of Gd- and Y-doped samples, remained unexplained. In this paper, we specifically devote our analysis to anomalies in the high-temperature regime, well above the spin-glass and metal-insulator transitions.

Differently from previous approaches in which *a*-RE_xSi_{1-x} alloys were considered as completely disordered, heavily doped magnetic semiconductors, we suggest that recent detailed conductivity and tunneling measurements clearly demonstrated the coexistence of metallic and semiconducting domains, identifying the percolative nature of electron transport in these systems.[5] Moreover, the role of short-range structural and magnetic order was not seriously discussed before, while, as a rule, different kinds of disorder exist in amorphous alloys.[9] The structural and compositional disorder at the atomic-scale distances can be qualitatively described within a model of point defects in a regular crystal lattice. Experiments indicate, however, that the disorder at the nanoscale distances has to be described differently, within a model of continuous defects with short-range order, embedded into a disordered effective medium (matrix).

It was proposed[10] that two different kinds of structural and magnetic disorder coexist in these systems, resulting, respectively, from isolated RE ions inside the *a*-Si host, and from nanoscale defects with enhanced concentration of RE ions, which cause a redistribution of the electron density, so that regions with higher electron concentration enveloping the nanoscale defects ("droplets") appear inside the matrix. Ferromagnetic ordering inside the droplets, more favorable than in the matrix, has been theoretically described within the "local phase transition" model.[11] To probe the magnetic state of the droplets, a "local" experimental method, electron paramagnetic resonance (EPR), was proposed, together with magnetoresistivity, Hall effect, and neutron-scattering measurements. Preliminary results[12–14] allowed for a crude estimate of some parameters of the droplets. As it was found for

a-Gd_xSi_{1-x}, e.g., with $x=0.14$, the typical droplet volume is $v_D \approx 400-800$ Å^3; the number of RE ions inside a droplet is $\kappa_D \approx 10-20$; the volume fraction occupied by the droplets is $f \approx 0.05-0.1$.

The paper is organized as follows. In Sec. II we analyze in detail the EPR measurement, preliminarily reported in Ref. 13. Here, we show that the experimental data can only be understood if the system finds itself in the so-called double-bottleneck regime, so that our proposal, that two subsystems (the matrix and the droplets) coexist, is crucial. In Sec. III we analyze in detail the magnetoresistivity and Hall effect experiments, previously reported in Refs. 12 and 14, providing further support in favor of our proposal of droplet formation. Here, we clearly demonstrate the percolative character of magnetotransport and the strongly inhomogeneous distribution of the magnetization in the system, provided by the formation of a network of droplets inside the matrix. In Sec. IV we summarize the results obtained in this paper and discuss their limit of validity, as well as the open problems. We also discuss the effect of the finite size of the droplets on their thermodynamics and explain the differences between the values of the droplet parameters calculated within our theory and those extracted from EPR and magnetotransport experiments. We finally explain the dependence of the critical temperature for the onset of short-range ferromagnetic order within the droplets on the alloy composition. In Appendixes A and B, for the sake of self-containedness, we briefly recall those aspects of our theoretical model[11] which are necessary to understand our interpretation of the experiments.

II. ELECTRON PARAMAGNETIC RESONANCE: EXPERIMENTAL RESULTS AND DISCUSSION

Electron paramagnetic resonance (EPR) is a powerful method to study the local spin arrangement in magnetic alloys, and is apt to detect the existence of droplets discussed above (see also Appendixes A and B). The complex magnetic properties of diluted a-Gd_xSi_{1-x} alloys were analyzed within ESR and Quantum Design superconducting quantum interference device (SQUID) dc magnetometry, as their composition x varied in the range $0.002 < x < 0.1$.[15] It was shown that Gd occurred in the trivalent state Gd^{3+} ($4f^7$, $S=7/2$, $L=0$), with a spectroscopic splitting factor close to $g=2$. The linewidth, determined as the field distance between peaks of the derivative of the absorption curve, was independent of the Gd concentration within the experimental accuracy and was $\delta B_{pp}=800\pm50$ G, at not too low temperature ($T>30$ K) and at the frequency $\nu=9.48$ GHz. Based on this result, the conclusion was drawn that the majority of Gd atoms enter into the composition of stable $GdSi_2$ complexes. The independence of the linewidth on the concentration of Gd ions is rather surprising, because, for example, the dipole-dipole broadening alone comprises more than 1.5 kG at an atomic concentration of about 10%; however, this circumstance was not explained at all in Ref. 15. The complete absence of any evidence for the fine structure, in spite of the definitely noncubic structure of $GdSi_2$ complexes and the high spin $S>1/2$, is also not clear.

Hereafter, the magnetic properties of a-Gd_xSi_{1-x} alloys are studied by means of EPR. The measurements were performed on an a-$Gd_{0.14}Si_{0.86}$ film 1.3 μm thick, fabricated by electron beam coevaporation onto a crystalline NaCl substrate.[17] The film area was about 10 mm^2. To perform the experiments, after dissolving the NaCl substrate, the film was fixed on a quartz holder installed in the goniometer of the resonator. The accuracy of adjusting the angle between the film plane and the magnetic-field direction was no worse than 0.5°. The spectra were recorded on a Bruker ESP-300 EPR spectrometer equipped with a helium-flow cryostat (Oxford Instruments). The experiments were carried out for $4\ \mathrm{K} < T < 300$ K at the frequency $\nu=9.46$ GHz, both for a magnetic field parallel and perpendicular to the film plane. Conventionally, the first derivative of the absorption signal was recorded.

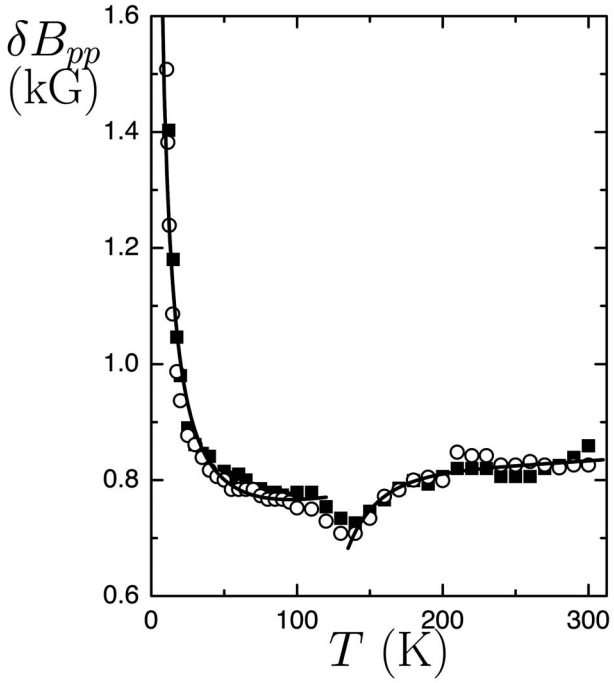

FIG. 1. Temperature dependence of the EPR linewidth δB_{pp} at the frequency $\nu=9.46$ GHz when the magnetic field is perpendicular (black squares) and parallel (open circles) to the film plane. The solid curves are obtained by Eqs. (28) and (29) for the optimal values of the fitting parameters (see text).

The absorption spectrum, observed for either orientation of the magnetic field, consisted of a single line. At $T \geqslant 30$ K, the line shape was fairly Lorentzian. As T was lowered below 30 K, the line shape changed, becoming close to a Gaussian at $T \leqslant 20$ K. The linewidth δB_{pp} (see Fig. 1) depended rather weakly on the temperature, in the region $T \geqslant 50$ K, and was about 800 G, as in Ref. 15. However, at variance with Ref. 15, a minimum in the linewidth, about 100 G deep, was found in the data analyzed in this work, in the temperature range 120–180 K. As T was decreased below 50 K, the line broadened rapidly, and its observation became impossible at $T \approx 5$ K. The resonance field for both orientations (see Fig. 2), at $T \geqslant 100$ K, decreased almost linearly with increasing T. The field strength for the perpendicular orientation was higher over the entire temperature range under investigation. This separation increased

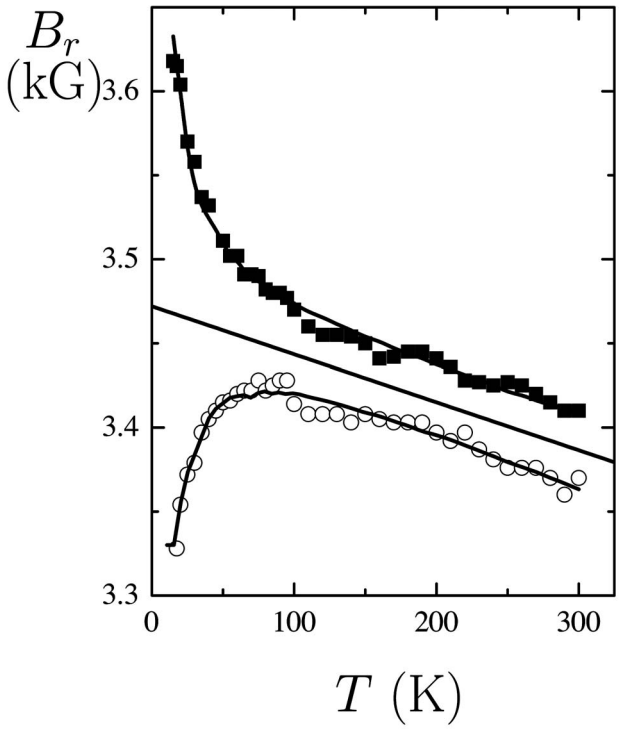

FIG. 2. Temperature dependence of the resonance-field strength B_r at the frequency ν=9.46 GHz, when the magnetic field is perpendicular (black squares) and parallel (open circles) to the film plane. The solid curves are obtained by Eq. (34) with the parameters B_0=3470 G, ξ=0.95, or ξ=−0.7 for the magnetic field perpendicular or parallel to the film plane, respectively, and ℓ=−0.3 G/K. The solid straight line corresponds to ξ=0.

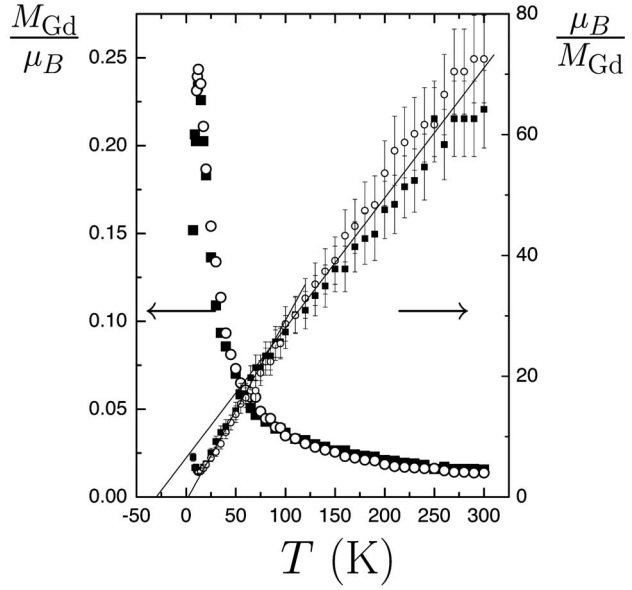

FIG. 3. Temperature dependence of the magnetic moment per Gd ion in the resonance field $M_{\rm Gd}$, for two orientations of the magnetic field with respect to the film plane. The symbols for the experimental points have the same meaning as in Figs. 1 and 2. The solid straight lines correspond to the Curie-Weiss law $M_{\rm Gd}^{-1}\sim T-\theta$.

with decreasing T, and reached a value $B_{r\perp}-B_{r\|}\approx 300$ G at $T\approx 10-15$ K. At $T\approx 300$ K, the orientation-averaged field strength corresponded to a g factor close to 2. The magnetic susceptibility, obtained by a double integration of the spectra, satisfactorily obeyed the Curie-Weiss law $\chi=C/(T-\theta)$ at $T\geqslant 100$ K, with a small negative Curie temperature $\theta\approx -30$ K. The absolute calibration of the susceptibility was performed in this region, where we took $C=S(S+1)g_{\rm Gd}^2\mu_B^2 n_{\rm Gd}(3k_B)^{-1}$. Here, $S=7/2$, $g_{\rm Gd}=2$, and $n_{\rm Gd}=7\times 10^{21}$ cm^{-3} are the spin, the g factor, and the concentration of Gd ions, respectively; μ_B is the Bohr magneton and k_B is the Boltzmann constant. In Fig. 3, the susceptibility is expressed in terms of the magnetic moment per Gd ion in the resonance field. As T was reduced below 100 K, θ decreased in absolute value, and even became positive ($\approx$5 K). The susceptibility itself reached a maximum at $T\approx 12$ K, and then sharply dropped. As it is known,[18] the sign of the Ruderman-Kittel-Kasuya-Yosida (RKKY) interaction depends on the electron concentration and on the distance between Gd ions. For inhomogeneous systems, the change in the sign of θ can be due to a change in the relative contribution to the susceptibility from the regions with ferromagnetic and antiferromagnetic interactions.

There are several sources of the EPR signal in the system under study: Gd ions residing in the matrix and in the droplets with higher electron concentration, as well as electrons. The Gd ions experience a noncubic crystal field that must lead to the fine splitting of the line since $S=7/2>1/2$. The absence of signals of various types, the absence of the fine structure, and the Lorentzian line shape, indicate that the double-bottleneck (DBN) conditions are fulfilled.[19] In this case, first, the exchange interaction of Gd ions with electrons leads to the disappearance of the fine structure and of the separate signals from these ions and electrons inside each subsystem (droplets and matrix), and second, the interaction between subsystems is sufficiently strong to promote the formation of one common EPR signal. For the realization of the first condition it is necessary that the inequality

$$|(\mathcal{T}_{es}^{-1}+\mathcal{T}_{se}^{-1})+i\Lambda(\chi_e\omega_s+\chi_s\omega_e)|\gg|(\mathcal{T}_{eL}^{-1}-\mathcal{T}_{sL}^{-1})+i(\omega_e-\omega_s)| \tag{1}$$

is fulfilled in each subsystem.[19] Here

$$\mathcal{T}_{es}^{-1}\approx\frac{8\pi x}{3\hbar}S(S+1)\varrho\mathcal{J}^2, \tag{2}$$

$$\mathcal{T}_{se}^{-1}\approx\frac{4\pi}{\hbar}(\varrho\mathcal{J})^2k_BT, \tag{3}$$

are the relaxation rate of electrons on ions (Overhauser relation), and the Korringa relaxation rate of ions on electrons, respectively; $\mathcal{T}_{eL}^{-1}$ and $\mathcal{T}_{sL}^{-1}$ are the spin-lattice relaxation rates of electrons and ions; χ_e and χ_s are the spin susceptibilities of electrons and ions, per lattice site; ω_e, ω_s, g_e, and g_s are the resonance frequencies and g factors of electrons and ions; x is the relative atomic concentration of magnetic ions, ϱ is the electron density of states (DOS) at the Fermi level per lattice site, $\mathcal{J}$ is the exchange-coupling constant between

itinerant electrons and Gd ions (see Appendixes A and B for detail);

$$\Lambda = \frac{2\mathcal{J}}{g_s g_e \mu_B^2} \tag{4}$$

is the molecular field constant. Then, for each subsystem, a single line is observed at a complex frequency

$$\omega \approx \frac{\chi_s \omega_s + \chi_e \omega_e}{\chi_s + \chi_e}, \tag{5}$$

where

$$\omega_s \approx \omega_s^0 + i\left(\mathcal{T}_{sL}^{-1} + \frac{M_2}{3\mathcal{T}_{se}^{-1} + i\Lambda\chi_e\omega_s^0}\right), \tag{6}$$

$$\omega_e \approx \omega_e^0 + i\mathcal{T}_{eL}^{-1}. \tag{7}$$

ω_s^0 and ω_e^0 are the bare resonance frequencies of isolated Gd spins and electrons, disregarding their interactions with the lattice and with each other; M_2 is the second spectral moment of magnetic ions due to nonisotropic spin-spin interactions, fine and hyperfine structures, and other sources of inhomogeneous broadening; a necessary condition for the applicability of Eq. (6) is

$$|3\mathcal{T}_{se}^{-1} + i\Lambda\chi_e\omega_s^0| \gg \sqrt{M_2}. \tag{8}$$

Let us estimate the quantities appearing in Eq. (1), and find a temperature range in which the bottleneck regime is possible. As we point out in Appendix A, the trivalent Gd^{3+} ion acts as a one-electron donor in the *a*-Si matrix. Assuming a Si concentration $n_{Si} \approx 5 \times 10^{22}$ cm^{-3} (Refs. 14 and 17) and for a relative Gd concentration, e.g., $x=0.14$, one can estimate the DOS within the simplest free-electron model, $k_B\varrho \approx 10^{-5}$ K^{-1}. The characteristic value of the exchange integral for RE elements is $|\mathcal{J}|/k_B \approx 10^3$ K. The electron and ion susceptibilities can be estimated by means of the well-known expressions

$$\chi_e \approx \tfrac{1}{2} g_e^2 \mu_B^2 \varrho, \tag{9}$$

$$\chi_s \approx \frac{xS(S+1)g_s^2\mu_B^2}{3k_BT}. \tag{10}$$

For $g_e \approx g_s \approx 2$ and a resonance field $B_r \approx 3.4$ kG, one may set $\omega_e \approx \omega_s \approx 2\pi \times 10^{10}$ s^{-1}. Now, by means of Eqs. (2)–(4), (9), and (10) we obtain the estimates $\mathcal{T}_{se}^{-1} \approx 10^8 T$ s^{-1}, $\mathcal{T}_{es}^{-1} \approx 3 \times 10^{13}$ s^{-1}, $|\Lambda\chi_e\omega_s| \approx 5 \times 10^8$ s^{-1}, and $|\Lambda\chi_s\omega_e| \approx 10^{14} T^{-1}$ s^{-1}. In the last expressions T must be expressed in K. It is clear that at $T \ll 10^5$ K, i.e., in the entire temperature range under investigation, $\mathcal{T}_{se}^{-1} \ll \mathcal{T}_{es}^{-1}$, $\chi_e \ll \chi_s$, and $|\chi_e\omega_s| \ll |\chi_s\omega_e|$. Besides, if T is not below 5 K, the inequalities

$$\mathcal{T}_{se}^{-1} > |\Lambda\chi_e\omega_s|, \tag{11}$$

$$\mathcal{T}_{es}^{-1} > |\Lambda\chi_s\omega_e| \tag{12}$$

hold, and hence $\mathcal{T}_{es}^{-1} + \mathcal{T}_{se}^{-1} > |\Lambda(\chi_s\omega_e + \chi_e\omega_s)|$. The simultaneous fulfillment of this inequality and of Eq. (1) sets the conditions for the so-called relaxation-dominated bottleneck (RBN). Let us assume that the inequality

$$\mathcal{T}_{eL}^{-1} \gg \mathcal{T}_{sL}^{-1} \tag{13}$$

for spin-lattice relaxation rates is fulfilled. Then, in view of Eqs. (8) and (11), and of the condition $\chi_e \ll \chi_s$, by means of Eqs. (6) and (7), Eq. (5) yields for the resonance frequency the expression

$$\omega \approx \omega_s^0\left(1 + \frac{M_2\Lambda\chi_e}{9\mathcal{T}_{se}^{-2}}\right) + i\left(\mathcal{T}_{sL}^{-1} + \frac{M_2}{3\mathcal{T}_{se}^{-1}} + \frac{\chi_e}{\chi_s}\mathcal{T}_{eL}^{-1}\right), \tag{14}$$

the real and imaginary part determining, respectively, the line position and width. The effective relaxation rate corresponding to the experimentally measured linewidth $\delta B_{pp} \approx 800$ G is[20] $\mathcal{T}_{\mathrm{eff}}^{-1} \approx \sqrt{3} g \mu_B \delta B_{pp}/(2\hbar) \approx 10^{10}$ s^{-1}. Each term in the imaginary part of Eq. (14) cannot exceed this value. For $\mathcal{T}_{eL}^{-1}$ this restriction reads $\mathcal{T}_{eL}^{-1} < 10^{15} T^{-1}$ s^{-1}. Thus, in the temperature range under investigation, the rate $\mathcal{T}_{eL}^{-1}$ can exceed both $M_2/(3\mathcal{T}_{se}^{-1})$ and $\mathcal{T}_{sL}^{-1}$, and a single restriction to its value can be imposed by the requirement (1). In view of the estimates carried out so far, each subsystem will be in the RBN regime if

$$\mathcal{T}_{eL}^{-1} < \mathcal{T}_{es}^{-1} \approx 3 \times 10^{13} \text{ s}^{-1}. \tag{15}$$

DBN conditions are fulfilled for subsystems, each of which is in the RBN regime, if an additional inequality is satisfied,[19]

$$\frac{\mathcal{T}_{eM}^{-1}\mathcal{T}_{De}^{-1} + \mathcal{T}_{eD}^{-1}\mathcal{T}_{Me}^{-1}}{\mathcal{T}_{eM}^{-1} + \mathcal{T}_{eD}^{-1}} \gg |\omega_M - \omega_D|, \tag{16}$$

where, henceforth, the subscripts M, D refer to the matrix and the droplets, that represent the two subsystems for Gd ions. When this condition holds, the complex frequency of the common resonance is determined by an expression similar to Eq. (5),

$$\omega^* \approx \frac{\chi_M\omega_M + \chi_D\omega_D}{\chi_M + \chi_D}. \tag{17}$$

The electron DOS in the droplets ϱ_D is higher than the DOS in the matrix ϱ_M. The ratio $\varrho_D/\varrho_M \approx 3.6$ is obtained in Appendix B for a reasonable value of the parameters, considering that the volume fraction occupied by the droplets is approximately $f \approx 0.1$ and the ratio of the total concentrations of Gd atoms in the droplets and in the matrix is $x_D/x_M \approx f\gamma/(1-f\gamma) \approx 0.5$, where $\gamma \approx 3.34$ is the enhancement factor measuring the ratio between the concentration of Gd ions in the droplets and their nominal concentration (see Appendixes A and B). These values will also be used below for various estimates. The left-hand side of Eq. (16), once the relations among the parameters ϱ and x is taken into account, reduces to $\approx 5\mathcal{T}_{Me}^{-1}$. In view of Eqs. (8) and (11), by means of Eq. (5), it is easy to obtain $|\omega_M - \omega_D| \approx 5 \times 10^{-6} T \mathcal{T}_{eL}^{-1}$ and the inequality (16) becomes $\mathcal{T}_{eL}^{-1} < 10^{14}$ s^{-1}. The last requirement is even weaker than the RBN condition (15).

Taking the real and imaginary parts of Eq. (17), we obtain, with the help of Eq. (14), the expressions for the line position and width,

$$\omega_r = \mathrm{Re}\ \omega^* \approx \omega_s^0 \left\{ 1 + \frac{\Lambda}{\chi_M + \chi_D} \left[\frac{(1-f)M_{2M}\chi_{e,M}\chi_M}{9\mathcal{T}_{Me}^{-2}} + \frac{fM_{2D}\chi_{e,D}\chi_D}{9\mathcal{T}_{De}^{-2}} \right] \right\}, \tag{18}$$

$$\delta\omega = \mathrm{Im}\ \omega^* \approx \mathcal{T}_{sL}^{-1} + \frac{(1-f)\chi_{e,M} + f\chi_{e,D}}{\chi_M + \chi_D}\mathcal{T}_{eL}^{-1} + \frac{1}{\chi_M + \chi_D}\left(\frac{M_{2M}\chi_M}{3\mathcal{T}_{Me}^{-1}} + \frac{M_{2D}\chi_D}{3\mathcal{T}_{De}^{-1}} \right). \tag{19}$$

By virtue of Eqs. (8) and (11), the line shift determined by Eq. (18) turns out to be much smaller than the Knight shift[19] $|\Delta\omega_r/\omega_s^0| \ll |\Lambda\chi_e| \approx |\varrho\mathcal{J}| \approx 10^{-2}$, and according to Eq. (3), the shift rapidly decreases with increasing T. In the second term of Eq. (19), the numerator does not depend on T and the denominator involves the total susceptibility $\chi_{\mathrm{exp}} = \chi_M + \chi_D$, which is inversely proportional to T to a rather good accuracy (see Fig. 3). Hence, similar to the Korringa relaxation, this term must make a contribution proportional to T to the linewidth. The form of the temperature dependence and, correspondingly, the contribution of the third term to the line width are determined by the ratio of the second moments and susceptibilities of the subsystems and can qualitatively differ in different temperature ranges.

Since the electron concentration is relatively small, the interaction of Gd ions in the matrix will be considered weak over the entire temperature range; therefore for these ions

$$\chi_M \approx \frac{x_M S(S+1) g_s^2 \mu_B^2}{3k_B T}. \tag{20}$$

In agreement with the model developed in Ref. 11 (see Appendix B for detail), a local ferromagnetic transition takes place in the droplets at $T = T_D$, given by Eq. (B2). Therefore for $T > T_D$ in the high-temperature paramagnetic phase, we assume that the Gd susceptibility in the droplets is

$$\chi_{D,HT} \approx \frac{x_D S(S+1) g_s^2 \mu_B^2}{3k_B (T - T_D)}. \tag{21}$$

In the low-temperature region $T < T_D$, the droplets containing κ_D Gd ions will be considered as superparamagnetic particles with spin $\kappa_D S$. The interaction between them, as well as between separate Gd ions in the matrix, is realized through electrons with DOS ϱ_M; therefore, similar to Eq. (20), their susceptibility can be estimated as

$$\chi_{D,LT} \approx \frac{x_D S(\kappa_D S + 1) g_s^2 \mu_B^2}{3k_B T}. \tag{22}$$

The distinction of the subsystems in the paramagnetic region at $T > T_D$ is mainly determined by the difference in the electron DOS, which does not directly affect M_2; therefore in this temperature range we take

$$M_{2,M} \approx M_{2,D} \equiv M_2. \tag{23}$$

As T approaches T_D, the relative contribution to the linewidth from the droplets increases in agreement with Eqs. (20) and (21). Because of the relations (3) and (23), and since $\varrho_D > \varrho_M$, the contribution to the linewidth from the third term in Eq. (19) decreases. Let us estimate the ratio of the second moments for $T < T_D$, assuming that the main contribution to the M_2 is due to a uniaxial anisotropy of the crystal field[21]

$$\mathcal{H}_1 = -\mathcal{D}(3\cos^2\phi - 1)S_z^2, \tag{24}$$

where ϕ is the angle between the direction of the magnetic field and the local z axis of a crystallite and S_z is the spin component. Under the assumption of a random distribution of the local z axes, the value of the second moment of Gd ions situated in the matrix, in the paramagnetic phase, is (see, e.g., Ref. 22)

$$\hbar^2 M_{2,M} \approx \frac{8\mathcal{D}^2}{15}\left[S(S+1) - \frac{3}{4} \right]. \tag{25}$$

The interaction of the κ_D ferromagnetically ordered spins in the droplet with the crystal field of Eq. (24) may be cast in the form

$$\mathcal{H}_D = -\sum_{j=1}^{\kappa_D} \mathcal{D}(3\cos^2\phi_j - 1)S_z^2 = -\frac{1}{\kappa_D^2}\sum_{j=1}^{\kappa_D} \mathcal{D}(3\cos^2\phi_j - 1) \times (\kappa_D S_z)^2 \equiv -\mathcal{D}_K S_{K,z}^2. \tag{26}$$

The mean square of $\mathcal{D}_K$, mediated over the sample, is equal to

$$\langle \mathcal{D}_K^2 \rangle = \left\langle \left[\frac{1}{\kappa_D^2}\sum_{j=1}^{\kappa_D} \mathcal{D}(3\cos^2\phi_j - 1) \right]^2 \right\rangle = \frac{4\mathcal{D}^2}{5\kappa_D^3}. \tag{27}$$

Then, we may apply Eq. (25) to estimate $M_{2,D}$. Assuming $\kappa_D \gg 1$ and using Eqs. (26) and (27), the *decision ratio* in the temperature range under consideration is $M_{2,D}/M_{2,M} \approx \kappa_D^{-1}$. Relying on Eqs. (3), (9), and (19)–(23), we obtain

$$\delta B_{pp,HT} = \delta B_{sL} + \frac{b_{HT}}{\chi_{\mathrm{exp}}} + \frac{\mathcal{P}}{T}\left[\left(1 + \frac{x_D}{x_M}\frac{T}{T - T_D} \right)^{-1} + A^{-2}\left(1 + \frac{x_M}{x_D}\frac{T - T_D}{T} \right)^{-1} \right] + \delta B_0, \tag{28}$$

in the high-temperature regime ($T > T_D$), and

$$\delta B_{pp,LT} = \delta B_{sL} + \frac{b_{LT}}{\chi_{exp}} + \frac{\mathcal{P}\mathcal{Q}}{T} + \delta B_0, \tag{29}$$

in the low-temperature regime ($T < T_D$). Here, $A \equiv \varrho_D/\varrho_M$ is the ratio between the DOS at the Fermi level in the droplets and in the matrix (see Appendix B),

$$\delta B_{sL} = \frac{2}{\sqrt{3}}\frac{\hbar}{g\mu_B \mathcal{T}_{sL}} \tag{30}$$

is the broadening due to spin-lattice relaxation,

$$b_{HT(LT)} = \frac{\hbar\mu_B g_e^2 \varrho_M [1 + f(A-1)]}{\sqrt{3} g \mathcal{T}_{eL}}, \tag{31}$$

$$\mathcal{P} = \frac{\hbar^2 M_2}{6\pi\sqrt{3} g \mu_B k_B (\varrho_M \mathcal{J})^2}, \tag{32}$$

$$\mathcal{Q} = \left(1 + \frac{x_D}{x_M}\frac{S}{S+1}\right)\left(1 + \frac{x_D}{x_M}\frac{\kappa_D S}{S+1}\right)^{-1}, \tag{33}$$

and δB_0 describes the line broadening due to all other mechanisms that were neglected in our model.

The solid lines in Fig. 1 correspond to Eqs. (28) and (29) with $\delta B_{sL} + \delta B_0 = 607$ G, $b_{HT} = 8 \times 10^{-5}$ μ_B, $b_{LT} = 12 \times 10^{-5}$ μ_B, $\mathcal{P} = 56\,562$ K G, $T_D = 137$ K, $\mathcal{Q} = 0.134$, $x_D/x_M = 0.5$, $A = 3.6$. The last two parameters were estimated in Refs. 11, 12, and 14 (see also Appendix B), and the other parameters were selected by a least-squares fit. It is evident that the experimental curves are rather well described by Eqs. (28) and (29): the deviation does not exceed the scatter of the experimental points in the entire temperature range except for the narrow region $120\ \mathrm{K} < T < 130\ \mathrm{K}$ (see Sec. IV for a discussion). The g factor in Eqs. (30)–(32) is determined from the value of the resonance field disregarding its shift due to the demagnetization effect associated with the shape of the sample. As will be shown below, it can be assumed that $g = 2$ with an accuracy not worse than 2–3 %, and $\varrho_M \mathcal{J} \approx -2.5 \times 10^{-2}$ can be estimated from the line shift extrapolated for $T \to 0$. As previously, we take $k_B \varrho_M \approx 10^{-5}\ \mathrm{K}^{-1}$. The g factor for electrons usually differs only slightly from $g_e = 2$ (the accuracy of this assertion will be estimated after the evaluation of $\mathcal{T}_{eL}^{-1}$). Now, Eqs. (30)–(33) lead to the estimates: $\mathcal{T}_{sL}^{-1} \leqslant 10^{10}\ \mathrm{s}^{-1}$, $\mathcal{T}_{eL}^{-1} \approx 10^{12}\ \mathrm{s}^{-1}$, $\hbar^2 M_2 / k_B^2 \approx 0.16\ \mathrm{K}^2$, and $\kappa_D \approx 24$.

It is evident that the assumptions (13) and (15) for the relaxation rates are well fulfilled. Moreover, the inequality (8) is fulfilled rather well at $T > 10$–20 K; hence, the system finds itself in the RBN, and Eqs. (5) and (17)–(19) are fully justified. From electrical conductivity data[12] it is possible to estimate the typical electron relaxation rate for momentum, $\mathcal{T}_R^{-1} \approx 10^{15} - 10^{16}\ \mathrm{s}^{-1}$. The deviation of the electron g factor from $g = 2$ is $\Delta g_e \approx \sqrt{\alpha \mathcal{T}_R / \mathcal{T}_{eL}}$, where $\alpha \approx 0.1$.[23,24] It follows that $\Delta g_e \leqslant 10^{-2}$, and this inequality assesses a precision for the proximity of the electron g factor to 2.

For a specified concentration of Gd ions, the second moment, conditioned by the dipole-dipole interaction, can be estimated as $\hbar^2 M_{2,dd} / k_B^2 \approx 0.024\ \mathrm{K}^2$, which is almost an order of magnitude smaller than the estimate that was obtained here for the total M_2. This circumstance explains the independence of the linewidth on the Gd concentration up to an atomic concentration of 10–20 %, and allows for the inference that the single-ion contribution to the resulting value of M_2 dominates. In other words, the main contribution to M_2 is not associated with the interaction of Gd ions with each other but is due either to their interaction with the nearest local environment, e.g., crystal field, or to hyperfine interaction. The hyperfine coupling constants for ^{155}Gd and ^{157}Gd are sufficiently small[25,26] and yield a splitting ≈ 3–5 G, that is much less than the characteristic linewidth. Moreover, the total relative natural concentration of the two isotopes is less than 30%. Thus, it is most likely that the second moment is conditioned by the crystal field of the nearest neighbors only.

Under the assumption of a uniaxial anisotropy, Eq. (24), the parameter $\mathcal{D}/k_B \approx 0.14$ K can be readily estimated by means of Eq. (25) [for $S = 7/2$, Eq. (25) gives $\hbar^2 M_2 \approx 8\mathcal{D}^2$].

The change in the resonance field with decreasing T can be related, among other things, to the increase of the sample magnetization $\mathcal{M}$.[27] It depends on the shape of the sample and on the arrangement of the ions—the sources of the EPR signal—in the crystal-lattice. For ions located at the crystal-lattice sites of a cubic symmetry, and also in the case of their isotropic random arrangement, the additional shift of the resonance field for the observation of EPR in a thin film equals $\Delta B_{r\perp} = 4\pi\mathcal{M}$ for the magnetic field perpendicular to the film plane, and $\Delta B_{r\parallel} = -2\pi\mathcal{M}$ for the magnetic field parallel to the film plane. Accordingly, and taking into account the linear behavior, which is clearly seen at high temperatures, an attempt was made to describe the temperature dependence of the resonance field by the curve

$$B_r = B_0 + \xi(4\pi\mathcal{M}) + \ell T. \tag{34}$$

A comment on the meaning of the last term in the right-hand side of Eq. (34) is postponed to the end of this section.

The solid lines in Fig. 2 are obtained by Eq. (34), with $B_0 = 3470$ G, $\xi = 0.95$ or -0.7 for the magnetic field perpendicular or parallel to the film plane, respectively, and $\ell = -0.3$ G/K. The magnetization $\mathcal{M} = n_{\mathrm{Gd}} M_{\mathrm{Gd}}$ was recalculated directly from the susceptibility data (see Fig. 3). It is evident that the experimental curves are rather well described by Eq. (34). A significant difference of the value of ξ from $-1/2$ for the parallel orientation of the field most likely points to the occurrence of short-range order of a noncubic symmetry in the arrangement of Gd ions. This may indicate that the formation of droplets and the ordering of Gd ions inside these droplets are of a chemical nature. The straight line in Fig. 2 corresponds to $\xi = 0$, and characterizes the value of the resonance field without its shift due to the magnetization of the sample. This determination of the resonance field yields a more accurate estimate for the g factor. The value B_0 corresponds to the resonance field that would be observed at $T \to 0$ K. The g factor in this case is $g_0 = 1.95 < 2$. As was already mentioned, the line shape approaches a Gaussian as T decreases below 20 K. This fact points to the slowing down of exchange fluctuations and to the escape of the system from the bottleneck regime. The slowing down of exchange fluctuations is most likely related to the fact that the system is approaching a phase transition to a spin-glass state.[2–4] In our work, the occurrence of a phase transition is indicated by both the maximum of the susceptibility ($T_m \approx 12$ K) and the disappearance of the EPR signal at a lower temperature ($T_f \approx 5$ K). Under these conditions, electrons rather rapidly relax to the lattice and their magnetization has time to follow the instantaneous value of the internal field.[19] This leads to a shift of the resonance field (Knight shift), whose value is determined by the well-known equation $\Delta g/g = \Lambda\chi_e = (g_e/g)\varrho\mathcal{J}$. To an accuracy of a few tenths of a percent, the g factor for noninteracting Gd^{3+} magnetic ions does not differ from $g = 2$.[25] Hence, using the experimental value $\Delta g = g_0 - 2 = -0.05$, one can easily obtain the estimate $\varrho_M \mathcal{J} \approx -2.5 \times 10^{-2}$ used above and, assuming that

$\varrho_M k_B \approx 10^{-5}$ K^{-1}, the value of the exchange constant $\mathcal{J}/k_B \approx -2.5\times 10^3$ K.

We point out that the strongly linear dependence of the resonance field on T, as given by Eq. (34), is not completely clear. According to our model, in the strong bottleneck regime the line shift (18) should fall off as T^{-2}, i.e., faster than observed in correspondence of the linear variation of the resonance field. Such a T^{-2} variation can be easily obtained by taking the real part of Eq. (14). One possible reason for the disagreement is, in our opinion, the weakening of the inequality (8) in some temperature range. It is known that the ratio of the various terms in this inequality defines the narrowing of the linewidth due to exchange. In view of Eq. (11), the square of the narrowing factor defines in Eq. (14) the part of the Knight shift that is due to the displacement of the resonance field in the bottleneck regime. If the inequality (8) is not strictly fulfilled, the exchange narrowing of the line does not occur. Hence, the displacement of the resonance field should be of the order of the Knight shift, and this essentially implies a slower reduction of the line shift in the temperature range considered here. We thus suggest that the almost-linear dependence of the resonance field on the temperature is somehow accidental, and is possibly connected with a "gradual" inclusion of the Knight shift as the temperature is reduced.

III. MAGNETOTRANSPORT: EXPERIMENTAL RESULTS AND DISCUSSION

While the x-ray studies of the local structure of a-$(Gd,Y)_xSi_{1-x}$ showed the absence of fluctuations at macroscopic scales,[28] detailed conductivity and tunneling measurements[5] have clearly demonstrated the coexistence of metallic and semiconducting domains, identifying the percolative nature of electron transport and the strongly inhomogeneous character of these alloys at nanoscale distances.

In this section, we consider some interesting results of magnetotransport measurements that have been carried out in the temperature range 5–300 K, in magnetic fields up to 4 T, using Van der Pauw and the standard Hall bar technique, and discuss their correspondence to the predictions of our theory. We use the samples prepared in F. Hellman's laboratory by a technique described previously.[17] Films of a-$(Gd,Y)_xSi_{1-x}$, 100–500 nm thick, were grown by e-beam coevaporation on Si/SiN substrates.

We devote our analysis to the high-temperature regime, neglecting all phenomena related to the spin-glass and metal-insulator transitions, and assume that electron transport occurs through the conducting network, which is formed by metallic nanoclusters with enhanced Gd concentration enveloped by higher-density electron clouds (droplets), connected by semiconducting bridges with low Gd concentration. Experiments[6] showed that the electrical conductivity $\sigma(T)$ increases almost linearly with the temperature T in a-Y_xSi_{1-x} at $T>2$–5 K and in a-Gd_xSi_{1-x} at $T>50$–70 K. Within the framework of our model, we approximate $\sigma(T)$ in the paramagnetic phase by the expression $\sigma(T)=\sigma_p(T)\approx\sigma_0+\sigma_{itin,p}(T)$, where the "residual" conductivity σ_0 is almost independent of T and will not be discussed here. It may be associated, e.g., with the simple shunting of a principal conducting path by indirect hopping of electrons through the matrix, or, in a more complex scenario, with the indirect tunneling of electrons between metallic droplets across semiconducting bridges. The term $\sigma_{itin,p}(T)$ strongly depends on T and can be expressed in the standard form $\sigma_{itin,p}(T)=|e|n_{itin,p}(T)\nu_p(T)$, where $n_{itin,p}$ and $\nu_p(T)$ are the itinerant electron concentration and mobility in the paramagnetic state, respectively.

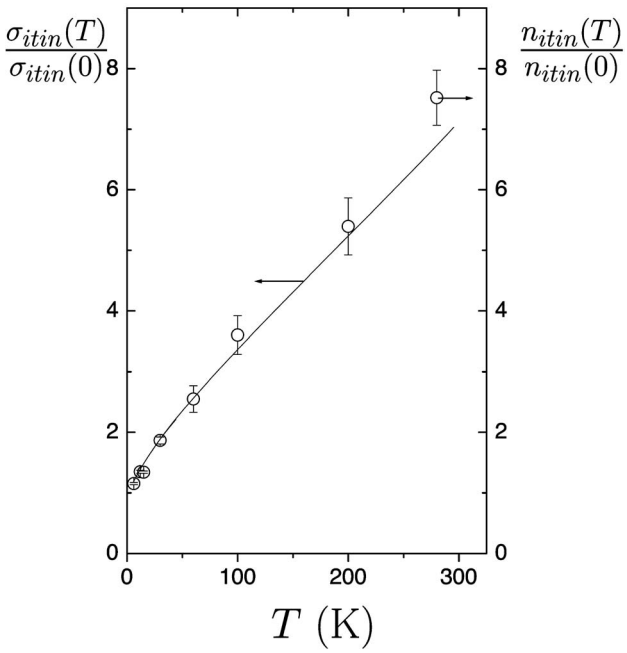

FIG. 4. Temperature dependence of the itinerant electron conductivity (solid line) and concentration (open circles) for nonmagnetic $Y_{0.17}Si_{0.83}$.

To clarify the role of $n_{itin,p}$ in the temperature dependence of the electrical conductivity, Hall-effect measurements were carried out. In Fig. 4, we present the experimentally determined $n_{itin}(T)\propto x_{itin,p}$ for nonmagnetic a-Y_xSi_{1-x}, which linearly increases with T, in the whole temperature range under investigation.[11,14] This implies that the dependence of $\nu_p(T)$ on T is weak enough, as resulting from the scattering of itinerant electrons on electrically neutral centers.[11,12,14] The temperature dependence of $\sigma_{itin,p}$ is obtained by taking into account the residual conductivity σ_0, which does not contribute to Hall effect. The data show that $\sigma_{itin,p}(T)/\sigma_{itin,p}(0)\approx n_{itin}(T)/n_{itin}(0)$ and confirm that the variation of $\sigma_{itin,p}(T)$ is produced by $n_{itin}(T)$, which increases linearly with T.

For the a-Gd_xSi_{1-x} magnetic alloys the increase of $\sigma_p(T)$ with T is strongly nonlinear for T below $\approx$50–70 K, and becomes quasilinear only above this temperature [see Fig. 5(a)]; we attribute this nonlinearity to complex magnetic transformations in the system. Consistently with the theory recalled in Appendixes A and B, short-range ferromagnetic order occurs in the form of ferromagnetic nanoscale defects enveloped by magnetically polarized higher-density electron clouds (droplets) at $T<T_D$ (where T_D is the temperature for the onset of local magnetic order, see Appendix B), in the

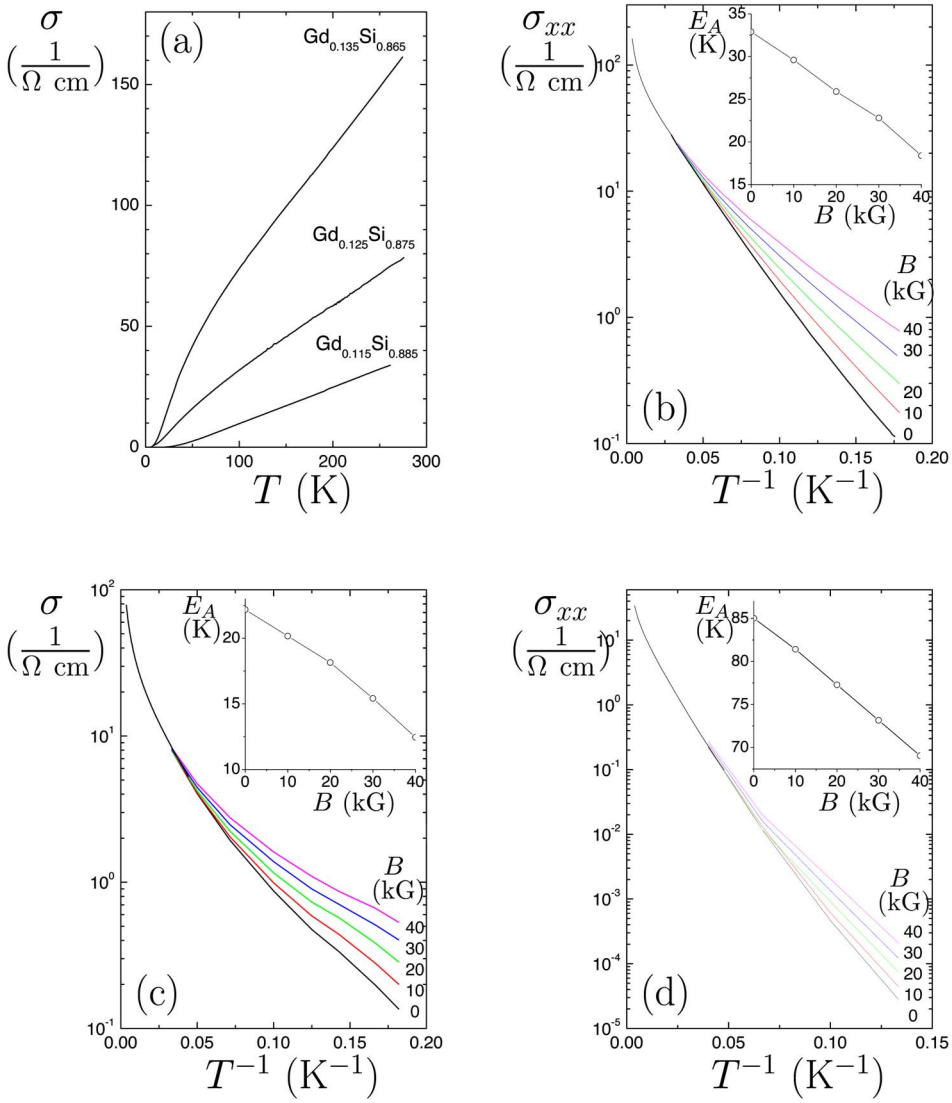

FIG. 5. (Color online) (a) Conductivity vs temperature dependence at zero-magnetic induction for Gd_xSi_{1-x} samples. Conductivity vs inverse-temperature dependence at various magnetic inductions for (b) $Gd_{0.135}Si_{0.865}$; (c) $Gd_{0.125}Si_{0.875}$; (d) $Gd_{0.115}Si_{0.885}$. The activation energy as a function of the magnetic induction is shown in the insets.

alloys containing magnetic Gd ions. We write now $\sigma(T) = \sigma_f(T) \approx \sigma_0 + \sigma_{itin,f}(T)$, where the subscript f denotes here the phase with short-range ferromagnetic order in the droplets, and is adopted for the sake of clarity. Two factors modify the temperature dependence of $\sigma_f(T)$, as compared to that of $\sigma_p(T)$. First, the exchange scattering of electrons on the noncorrelated magnetic moments of the superparamagnetic droplets appears and shifts the electron mobility edge upwards, $\varepsilon_m \rightarrow \varepsilon_m + \Delta\varepsilon_m$, where $\Delta\varepsilon_m/\Gamma \sim \beta(T) \equiv \lambda(\mathcal{J}\kappa_D\langle S_z\rangle)^2/U^2$, λ is the ratio between the number of droplets and the number of Gd ions, and U is the potential which couples electrons to the local disorder component (see Appendixes A and B for detail). Thus the concentration of itinerant electrons $n_{itin,f}(T)$ is decreased for $T < T_D$.

Second, a dependence of the itinerant electron mobility $\nu_f(T)$ on T appears, which is qualitatively described as a superposition of the potential and exchange mechanisms for electron scattering on the disordered ferromagnetic droplets. Assuming that the characteristic droplet size is small, as compared to the electron mean free path, we estimate $\nu_f(T)/\nu_p(T) \sim 1 - \beta(T)$.

The parameter $\beta(T)$ is zero for $T > T_D$ and may vary in the range 0.01–0.1 for $T \ll T_D$, if $(\mathcal{J}S)^2/\langle U^2\rangle \approx 0.01$–$0.1$, $\kappa_D \approx 10$–20, $\lambda \approx 0.01$–0.03. From the data in Figs. 5(b)–5(d), we conclude that the variation of the itinerant electron concentration plays the major role in our system, and the variation of the mobility can be neglected. In any case, the appearance of short-range ferromagnetic order obviously enhances the tendency towards the metal-insulator transition.

Let us now discuss the variation of the conductivity $\sigma(B)$ in our system as a function of the average magnetic induction B. From Fig. 6, we see that at $T < 50$–70 K there are two regimes of magnetic fields characterized by a different behavior of $\sigma(B)$. At $B < B_C$, where B_C is a characteristic value, the conductivity only slightly depends on B. At $B > B_C$ an exponential dependence is observed. Moreover, B_C increases with increasing temperature. Notice that B_C is determined by the intersection of the local fit of the experimental $\ln[\sigma(B)/\sigma(B=0)]$, as a function of B, with the line $\ln[\sigma(B)/\sigma(B=0)] = 1$ at low temperatures. For high temperatures we use B_C as a scaling parameter.

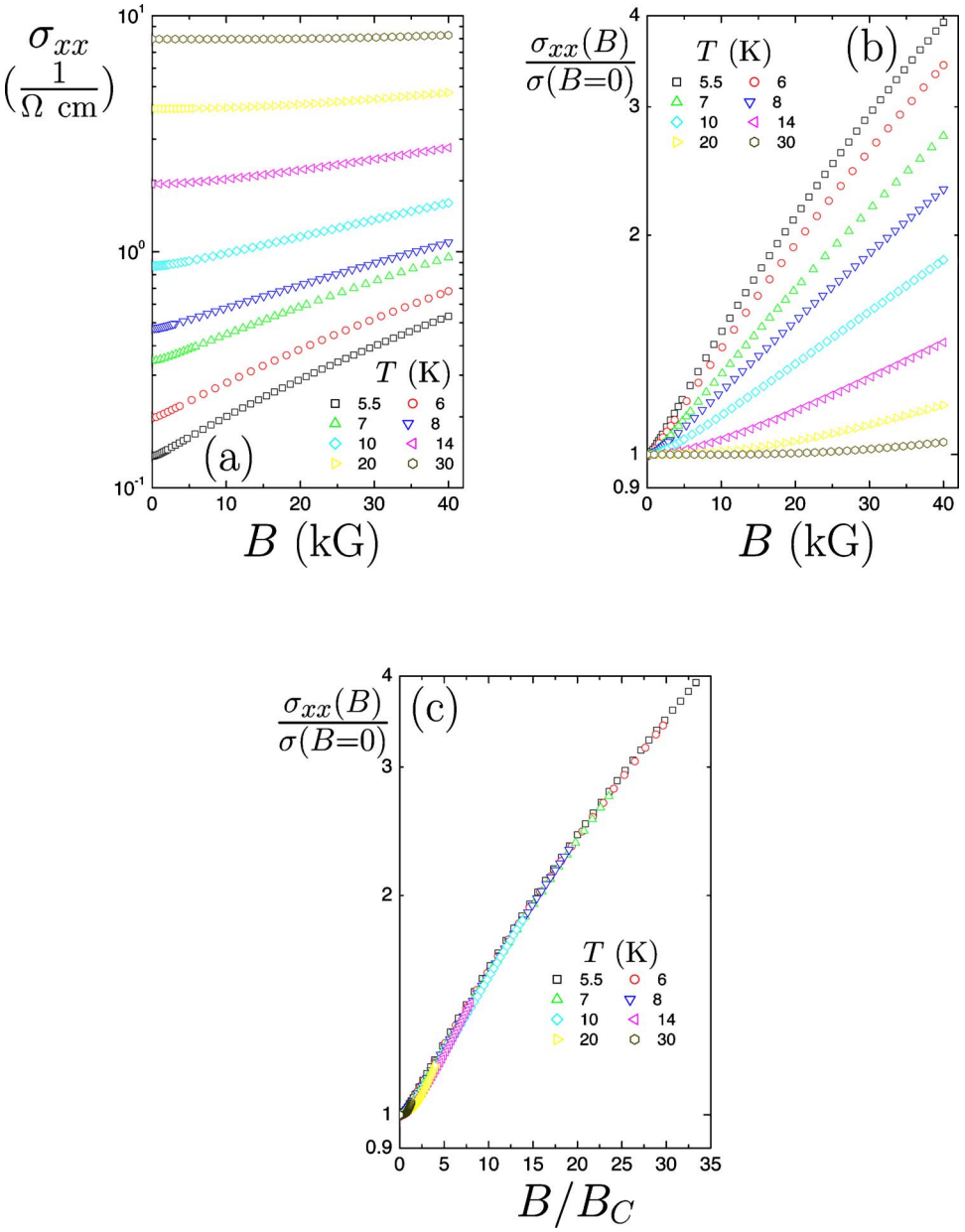

FIG. 6. (Color online) (a) Conductivity vs magnetic-induction dependence for $Gd_{0.125}Si_{0.875}$ at different temperatures; (b) the same dependence when the conductivity is rescaled by the zero-field value; (c) the same dependence when the magnetic induction is rescaled by the characteristic value B_C (see text) to put in evidence the data collapse.

Within the framework of our model of ferromagnetic droplets, we suppose that B_C corresponds to the field that aligns the magnetic moments of different droplets. At $B < B_C$, the magnetic energy of an isolated droplet $\kappa_D \langle S_z \rangle \mu_B g_{\mathrm{Gd}} B$ is smaller than the thermal energy $k_B T$, and therefore the magnetic moments of different droplets are disordered. This leads to an additional fluctuation potential in the system and raises the mobility edge, as discussed above. For $B > B_C$ the magnetic moments of different droplets are aligned and this scattering channel is eliminated. This effect reduces the mobility edge and increases the itinerant electron concentration, leading to an increase of the conductivity.

The value of the magnetic moment of the droplet obtained from the low-temperature part of the curve $B_C(T)$ allows us to roughly estimate the average number of Gd atoms in a droplet κ_D from the condition $\kappa_D \langle S_z \rangle \mu_B g_{\mathrm{Gd}} B_C \approx k_B T$. The experimentally determined function $\kappa_D \langle S_z \rangle / S = k_B T / (S \mu_B g_{\mathrm{Gd}} B_C)$ is shown in Fig. 7. At low T, when the saturation regime $\langle S_z \rangle \approx S$ is reached, we obtain $\kappa_D \approx 10$, which is in a range consistent with our theoretical predictions (see Appendix B), but is smaller than the value $\kappa_D \approx 24$ obtained from EPR measurements (see Sec. II). Note that all the experimental values of κ_D are close for different samples.

It should be noted that the dependence $\sigma(B)$ has a universal form for different temperatures. The experimental curves in Fig. 6, where the data for $\sigma(B)/\sigma(B=0)$ are plotted as functions of B/B_C for different temperatures, can be approximated at $B > B_C$ by the simple expression $\sigma(B)/\sigma(B=0)$

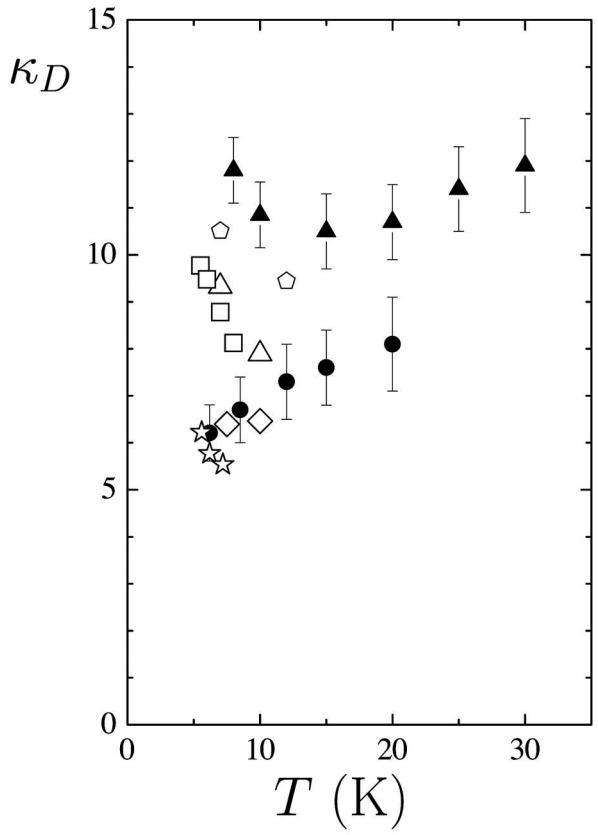

FIG. 7. Mean number of Gd ions in a droplet evaluated as a fitting parameter for the $B_{in}(B)$ dependence (shown in Fig. 8) through Eq. (37), for $Gd_{0.145}Si_{0.855}$ (filled triangles); $Gd_{0.16}Si_{0.84}$ (filled circles). The open symbols show the mean spin of a droplet in units of S, $\kappa_D\langle S_z\rangle/S$, experimentally determined as $\kappa_D\langle S_z\rangle/S = k_BT/(S\mu_B g_{Gd}B_C)$ at low temperatures (when $\langle S_z\rangle/S \approx 1$) for $Gd_{0.115}Si_{0.885}$ (diamonds); $Gd_{0.125}Si_{0.875}$ (squares); $Gd_{0.135}Si_{0.865}$ (stars); $Gd_{0.14}Si_{0.86}$ (pentagons); $Gd_{0.145}Si_{0.855}$ (triangles).

$\approx \exp(B/B_C - 1)$. This gives for the concentration of itinerant electrons at $B \gg B_C$,

$$\frac{n_{itin}(B)}{n_{itin}(B=0)} \approx \exp\left(\frac{B}{B_C}\right). \tag{35}$$

Our explanation of this result is the following. We suppose that the Zeeman splitting in the matrix leads to a downward (upward) shift of the bottom of the itinerant electron spin-up (spin-down) subband with respect to the Fermi level. At high B the full-splitting regime sets in, when the spin-down subband remains empty, the local Fermi energy measured from the bottom of the spin-up subband rises linearly with B. Within this assumption, the electron activation energy $E_A(B,T)$ may be easily obtained from the dependence of $\sigma(B,T)$. The slope of $\mathcal{M}_M \equiv \partial E_A/\partial B$ is proportional to the Zeeman splitting in the matrix and allows us to estimate the effective magnetization of itinerant electrons in the matrix. We analyzed the functions $\mathcal{M}_M(B,T)$ for various alloys in a wide range of values for B and T and concluded that, for a fixed alloy composition, they coincide at $B \gg B_C$, when the estimate (35) may be used. The values of $\mathcal{M}_M(B,T)$ vary in the range $(2-6)\mu_B$ for samples with different composition.

Thus our experiments have shown that a strong magnetic induction B suppresses the tendency towards the metal-insulator transition. This fact is naturally explained within the model developed in Refs. 11, 12, and 14, if we take into account the suppression of the electron-exchange scattering on the magnetic droplets, provided by their coherent orientation in the magnetic field. An exponential increase of the itinerant electron concentration $n_{itin}(B)$ with B is obviously caused by the spin-up subband lowering due to the Zeeman splitting at high field.

The interpretation exposed above for magnetotransport experimental results seems to be very rough, due to the strongly inhomogeneous spin-density distribution in the system, which was not taken into account. While the average (over the sample) magnetization in a-$(Gd,Y)_xSi_{1-x}$ alloys is very small and we estimate $B \approx H$, where H is the external magnetic field, the local magnetization inside the percolation network containing ferromagnetic droplets strongly differs from that in the matrix. As a result, the "internal" magnetic induction inside the conducting regions (B_{in}) may significantly exceed the average magnetic induction B.

In the following, we discuss in more detail the magnetic-field dependences of transverse (R_{xx}) and Hall (R_{xy}) magnetoresistances in our system. However, before analyzing the experimental results, an important remark is mandatory.

We assume that the conductivity in a-$(Gd,Y)_xSi_{1-x}$ alloys is primarily associated with electrons moving in wide bands formed by (s-p) hybridized Si orbitals. Each Gd ion enters into the matrix of a-Si in the form of a trivalent ion that closes the broken bonds between two neighboring Si ions, giving two electrons to saturate these bonds.[15] Owing to such a specificity of the chemical bond, the "anomalous" contribution to magnetotransport, due to the spin-orbit interaction between itinerant (s-p) states of Si and localized f states of Gd is likely to be not significant in a-$(Gd,Y)_xSi_{1-x}$.

For these reasons, we take into account only the "normal" component of R_{xy}, and assume that the components (R_{xx},R_{xy}) are related to the itinerant electron concentration and the "internal" magnetic induction inside the current-flowing regions as $1/R_{xx} \sim n_{itin}$, $R_{Hall} = R_{xy}/B_{in} \sim 1/n_{itin}$. Excluding n_{itin} from these equations, we can plot the dependence of $B_{in} \sim R_{xy}/R_{xx}$ on the external field $H \approx B$ in arbitrary units (see Fig. 8). It is seen that the dependence $B_{in}(H)$ is strongly nonlinear as a whole. However, in the region $H > 20$ kG it is almost linear and contains a constant contribution that, as we believe, is attributed to the saturation magnetization M_s of the sample. Taking into account the saturation of the magnetization in strong fields, we normalize the slope of the dependence of $B_{in}(H)$ for $H > 20$ kG to unity and thereby determine the absolute value of B_{in}. This method allows us to estimate the magnetization of the material, and also serves as a Hall magnetometer, sensitive to the local magnetization of the material in the region where the current flows.

From the approximate relation $B_{in}(H > 20\ \text{kG}) \approx H + 4\pi M_s^{exp}$, we can roughly estimate the experimental value of the saturation magnetization $M_s^{exp} \approx 2$ kG. As it can be easily shown, this value significantly exceeds the theoretical limit

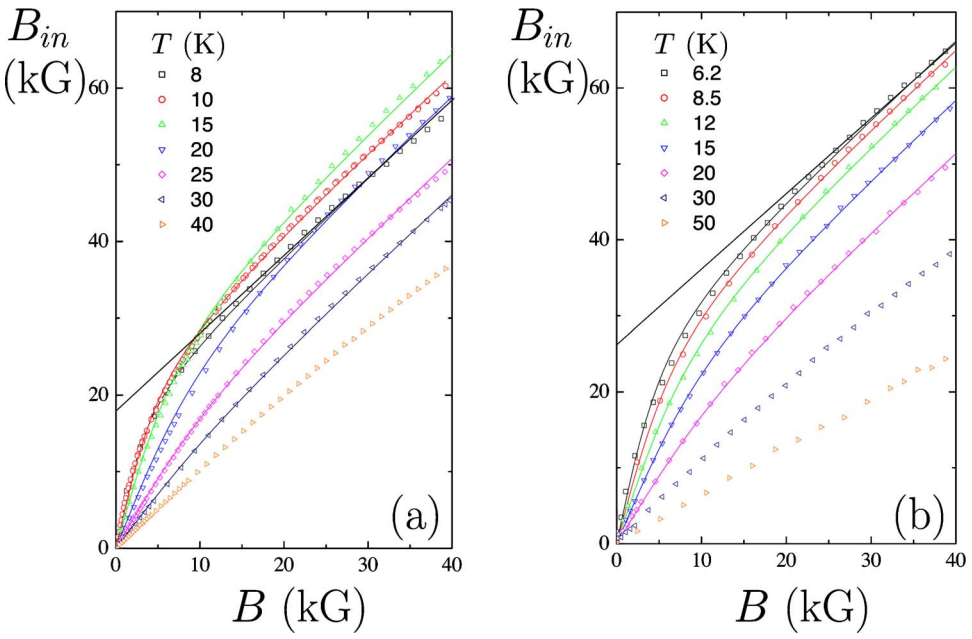

FIG. 8. (Color online) Local magnetic induction B_{in} inside the current-flowing regions vs average magnetic induction $B \approx H$ in (a) $Gd_{0.145}Si_{0.855}$ and (b) $Gd_{0.16}Si_{0.84}$ for various temperatures. The experimental data are normalized such that the slope of the asymptotic linear dependence is equal to one. The solid lines are obtained by Eq. (37). The resulting values for the fitting parameter κ_D are shown in Fig. 7.

M_s^{theo}, obtained under the naive assumption of a uniform distribution of Gd ions over the sample volume, $M_s^{theo} = n_{Gd}\mu_B S g_{Gd} \approx 450$ G. Thus, the simplest interpretation of the experimental results falls down, and a finer analysis of the situation is necessary.

Let us recall that electron transport in our system is of percolative nature and occurs trough the network, which is formed by droplets enveloping structural defects with an enhanced concentration of Gd ions. Thus the average magnetic induction B_{in} for the current that flows along the network may sizably differ from that in the matrix. For a thin-film sample, in the presence of an external magnetic field perpendicular to the film plane, we have

$$B_{in} = H_{in} + (4\pi - \eta_c)\mathcal{M}_c, \tag{36}$$

where $H_{in} = H - (8\pi/3)f\mathcal{M}_c$ is the average magnetic field inside the network, f is the volume fraction occupied by the droplets, η_c is the demagnetization coefficient, $\mathcal{M}_c = \mathcal{M}_{cs}\mathcal{L}(\kappa_D \mu_B S g_{Gd} H_{in}/k_B T)$ is the average magnetization inside the network, $\mathcal{M}_{cs} \approx n_{Gd}^{net}\mu_B S g_{Gd}$ is the saturation magnetization of the droplets, n_{Gd}^{net} is the average concentration of Gd ions in the network, $\mathcal{L}(y) = \coth(y) - 1/y$ is the Langevin function, and the semiclassic approximation is justified by the large value of the spin of the superparamagnetic particles. For randomly oriented droplets, which are not too anisotropic in shape, the approximation $\eta_c \approx 4\pi/3$ is reasonable. Taking into account that $f \ll 1$ in all a-Gd_xSi_{1-x} samples with $0.1 < x < 0.2$, we obtain $H_{in} \approx H$, and Eq. (36) can be recast in the form

$$B_{in} \approx H + \frac{8\pi}{3}\mathcal{M}_{cs}\mathcal{L}\left(\frac{\kappa_D \mu_B S g_{Gd} H}{k_B T}\right). \tag{37}$$

The solid lines in Fig. 8 are plotted according to Eq. (37), with κ_D and $\mathcal{M}_{cs}$ used as fitting parameters. It is seen that the experimental dependence $B_{in}(H)$ is well approximated by the model of the current that flows through ferromagnetic droplets; the value $\mathcal{M}_{cs} \approx 2.8$ kG is obtained for the saturation magnetization. Taking into account the range of possible values of the demagnetization factor $\eta_c = 0 - 2\pi$, we estimate the enhancement of the local density of Gd ions, $\gamma = n_{Gd}^{net}/n_{Gd} \approx 3 - 6$, which agrees with the value predicted by our theory (see Ref. 11 and Appendix B).

The parameter κ_D, obtained by using Eq. (37) to fit the experimental data, is compatible with that estimated from the temperature dependence of B_C (see Fig. 7). Notice that the saturation magnetization is approximately the same in samples with different compositions. Therefore, the concentration of Gd ions in the droplets is approximately the same as well. The magnetization of the matrix varies significantly for samples with different compositions, but remains too small, as compared to the magnetization of the droplets, to be detected.

IV. CONCLUSION

In this paper we devoted our analysis to the high-temperature regime of the a-RE_xSi_{1-x} alloys, i.e., far above the metal insulator and paramagnet to spin-glass transitions. Our theoretical approach is specifically appropriate to this regime. We did not discuss quantum corrections associated with electron correlations, weak-localization effects, and spin-glass freezing, which are relevant to explain transport properties at low temperature, and require a more refined model for the frequency dependence of the electron self-energy associated with disorder.

Our analysis of the EPR and transport properties of these alloys was based on the proposal that (i) the formation of nanoscale structural defects enriched with RE ions, enveloped by higher-density electron clouds (droplets), is promoted by the chemical tendency to the formation of stable $[RESi_2]_N$ complexes, and that (ii) when the RE has a nonzero spin, the conditions for the onset of short-range ferromagnetic order are met in the droplets, due to the higher electron density. In our proposal, the presence of ferromagnetic droplets in the magnetic a-Gd_xSi_{1-x} alloys plays a crucial role in the temperature regime under investigation and explains, e.g., the differences observed with respect to the nonmagnetic a-Y_xSi_{1-x} alloys. These differences cannot be justified, e.g., by electron-correlation effects, which would act in a similar way in both Gd- and Y-doped alloys.

The effective number of Gd ions inside the droplet (κ_D) and the typical droplet volume (v_D) were estimated under rather general theoretical assumptions[11] (see also Appendixes A and B). The full agreement with EPR (Sec. II) and magnetotransport (Sec. III) results is possible, taking into account the various assumptions of our interpretation and the experimental error bar. We point out that our theoretical results (recalled in Appendixes A and B) were obtained within the mean-field approximation, which may be not fully correct for the system under consideration.

First, we assumed that all the droplets are equal and homogeneously distributed within the matrix, while in real alloys droplets with different κ_D and v_D may coexist, and their spatial distribution may be inhomogeneous. If we suppose that the "rarefied" droplets with large v_D and small κ_D form continuous links of the conducting network, whereas the "concentrated" droplets with small v_D and large κ_D (i.e., large total spin $\kappa_D S$) form isolated superparamagnetic nanoparticles and play the main role in electron-spin relaxation, then it is easy to understand the partial discrepancy between the estimates obtained from EPR and magnetotransport results of Secs. II and III.

Second, analyzing these results, we assumed that the ferromagnetic transition in all the droplets takes place at the same mean-field temperature $T_D = T_D^{MF}$, and the magnetic moment of each droplet is set at once such as though all the spins in a droplet were strictly aligned in a ferromagnetic arrangement. However, even in the mean-field approach, there is a temperature range in which the spontaneous magnetization gradually grows from zero at $T = T_D$, up to saturation at $T \ll T_D$. Besides, the relatively small volume of the droplets enhances the role of spin fluctuations, which causes a spread in the temperatures of magnetic ordering in the region $\Delta T_D / T_D^{MF} \sim (r_D/a)^{-2}$ around T_D^{MF} (see, e.g., Ref. 29). For $T_D^{MF} \approx 100$K and $(r_D/a)^{-2} \approx 0.2$–0.4 we estimate $\Delta T_D \approx 20$–40K; therefore, in the transition region, one should not expect a full agreement between the experimental data and the mean-field model, the discrepancy between theory and experiment being quite natural.

As mentioned above, we identify T_D with the characteristic temperature T^*, below which the electrical conductivity sharply decreases with decreasing T, suggesting that the strongly nonlinear reduction of $\sigma(T)$ observed experimentally at $T < T^*$ is connected with complex magnetic transformations in the system, i.e., the appearance of short-range ferromagnetic order inside the droplets.

From our theoretical and experimental studies, we estimated the effective number of Gd ions κ_D in the characteristic volume v_D of the droplet, and found that the local composition of the droplet approximately corresponds to that of gadolinium disilicide, $GdSi_2$. In our opinion, this result reflects the "chemical" origin of the droplet and its stability in the form of a molecular complex, similar to $[GdSi_2]_N$, with $N \approx 10$–20.

It is evident that the dependence of T^* on the alloy composition gives very important information about the nature of the droplets. Experiments[6] revealed a strong decrease of $T^*(x)$ with increasing nominal Gd content x in the range $0.11 < x < 0.24$, which may be naturally explained in our model. In fact, one has to consider the various parameters that determine the local transition temperature T_D [see Eq. (B2) in Appendix B]. We assume that the droplet parameters (κ_D, v_D) depend only weakly on the nominal Gd concentration and are fixed by the conditions for the energy minimum of Gd-Si chemical bonds. Obviously, these parameters strongly depend on the details of the growing process. Within such an assumption, only the variation of the local DOS at the Fermi level ϱ_D leads to a change of T_D [see Eq. (B2)], with varying nominal Gd concentration. The potential φ_p [defined by Eq. (A2)], with the parameter $r_D \to r_{D,p}$ calculated in the paramagnetic phase, is proportional to the difference between the real and the nominal number of Gd ions within a droplet $\Delta\kappa = \kappa_D - \kappa$, i.e., it decreases when the nominal number κ of Gd ions in the droplet increases with increasing x. So, the local DOS at the Fermi level inside the droplet decreases and tends to that in the matrix. In our model of a semielliptic DOS, which is justified for a low density of carriers, this decrease is very strong,[11] and this obviously leads to a suppression of the local transition temperature T_D.

In brief, using our theoretical estimates and various experimental methods, we argued that nanoscale structural defects with a high concentration of RE ions enveloped by higher-density electron clouds (droplets) play an important role in a-RE_xSi_{1-x} alloys in a wide range of temperatures and magnetic fields. The existence of droplets with short-range ferromagnetic order well explains the EPR experiments on a-Gd_xSi_{1-x} discussed in Sec. II and the magnetotransport measurements on a-$(Gd,Y)_xSi_{1-x}$ discussed in Sec. III. It is also corroborated by neutron diffraction experiments,[12] in which ferromagnetic correlations with a correlation length ~ 5 Å have been observed, and the mean distance between Gd ions was estimated to be about 2 Å. Thus, we think that the a-RE_xSi_{1-x} alloys are new magnetic materials with unique properties of both strongly inhomogeneous compounds and nanocomposites.

ACKNOWLEDGMENTS

We are grateful to F. Hellmann and E. Helgren for sample preparation and critical remarks, and to C. Di Castro, C. Castellani, and M. Grilli, for valuable discussions. N. C., S. G., and V. T. were supported in part by the CRDF (Grant No.

RP2-2402-MO-02) and by the Grant RRC KI. V. T. was supported in part by the RFBR (Grant No. 04-02-16090). S. C. was supported by the Italian MIUR, Cofin 2003, prot. 2003020230_06 and Cofin 2005, prot. 2005022492_01.

APPENDIX A: THE MODEL FOR STRUCTURAL NANOSCALE DEFECTS

As stated in Sec. I the disorder in a-RE_xSi_{1-x} alloys at atomic-scale distances is associated with Si dangling bonds and isolated RE ions, within the a-Si network, similarly to all amorphous alloys, whereas at nanoscale distances it is associated with RE structural defects. Within a simplifying scheme, we describe the system as a set of nanoscale defects embedded into a weakly disordered matrix, which is quasihomogeneous over length scales larger than the interatomic distances, but smaller than the nanoscale-defect sizes and distances. We assume that the electronic structure of the matrix, averaged over the realizations of the atomic-scale disorder, may be described in terms of quasiperiodic electron states with a finite lifetime.

In Ref. 11, we adopted a one-band Hamiltonian

$$\mathcal{H} = \sum_{\mathbf{k},\alpha} E(\mathbf{k}) c^{\dagger}_{\mathbf{k},\alpha} c_{\mathbf{k},\alpha} + \int d\mathbf{r} \sum_{\alpha,\beta} [U_{\alpha\beta}(\mathbf{r}) + \Phi(\mathbf{r})\delta_{\alpha\beta}] \Psi^{\dagger}_{\alpha}(\mathbf{r}) \Psi_{\beta}(\mathbf{r}), \tag{A1}$$

where $\mathbf{k}$ is the quasimomentum, $E(\mathbf{k})$ is the ideal band dispersion, $c^{(\dagger)}_{\mathbf{k},\alpha}$ annihilates (creates) a band electron, with spin projection $\alpha=\uparrow,\downarrow$, and $\Psi^{(\dagger)}_{\alpha}(\mathbf{r})$ annihilates (creates) an electron at the point $\mathbf{r}$, with spin projection α. The local disorder potential is $U_{\alpha\beta}(\mathbf{r})=\Sigma_i(\mathcal{V}\delta_{\alpha\beta}+\mathcal{J}\vec{S}_i\cdot\vec{\sigma}_{\alpha\beta})\delta(\mathbf{r}-\mathbf{r}_i)$, where $\mathcal{V}$ and $\mathcal{J}$ are the Coulomb and exchange coupling with impurities, $\vec{S}_i$ is the local spin vector, and $\vec{\sigma}$ is the vector of Pauli matrices. The sum is carried over the random impurity sites $\mathbf{r}_i$. The continuous disorder potential, $\Phi(\mathbf{r})=\Sigma_j\Phi_j(\mathbf{r})$, where $\Phi_j(\mathbf{r})$ is the potential energy of an electron in the effective "envelope" Coulomb potential of the jth nanoscale defect, is sizable only inside the droplets. We take for simplicity $\Phi_j(\mathbf{r})=-\varphi$, independent of $\mathbf{r}$, inside the jth droplet, and zero elsewhere. Within this approximation, φ acts as a shift of the bulk chemical potential μ inside a droplet.

For the sake of clarity, we recall the droplet parametrization of Ref. 11. Hereafter, the subscripts D and M refer to droplets and matrix. N_D and N_M are the total numbers of RE ions in the two subsystems, the total number $N_{\mathrm{tot}}=N_D+N_M$ being fixed. The volume of the system is $V_{\mathrm{tot}}=V_D+V_M$, where V_D and V_M are the volumes of the two subsystems. The droplet volume fraction is $f\equiv V_D/V_{\mathrm{tot}}<1$. The RE concentration in the nanoscale defects is $n_D\equiv N_D/V_D=\gamma n$, where $\gamma>1$ is the enhancement factor, and $n\equiv N_{\mathrm{tot}}/V_{\mathrm{tot}}$ is the nominal concentration. Since $V_D=fV_{\mathrm{tot}}$, we have $N_D=f\gamma N_{\mathrm{tot}}$, $N_M=(1-f\gamma)N_{\mathrm{tot}}$, and from $V_M=(1-f)V_{\mathrm{tot}}$, we obtain the RE concentration in the matrix $n_M\equiv N_M/V_M=(1-f\gamma)n/(1-f)$. For simplicity, we take the droplets equal and spherical, with radius r_D and volume v_D. The number of RE ions in a single defect is $\kappa_D=n_Dv_D$ and the excess of RE ions with respect to the matrix is $\Delta\kappa\equiv(n_D-n_M)v_D=(\gamma-1)\kappa/(1-f)$, where $\kappa\equiv nv_D$ is the nominal number of RE ions in a defect. Thus we find $\gamma=1+(1-f)\Delta\kappa/\kappa$ and we take $\Delta\kappa$ and κ as parameters of our model with $\kappa_D=\gamma\kappa=\kappa+(1-f)\Delta\kappa$. Indicating with $\mathcal{N}_D$ the total number of droplets, we have $fV_{\mathrm{tot}}=V_D=\mathcal{N}_Dv_D$, i.e., $f=\mathcal{N}_Dv_D/V_{\mathrm{tot}}$. Assuming that the number of droplets per unit volume, $\mathcal{N}_D/V_{\mathrm{tot}}$, is fixed during the growing process, f turns out to be proportional to v_D, i.e., to κ. We write $f=\lambda\kappa$ with $\lambda\equiv\mathcal{N}_D/N_{\mathrm{tot}}$ taken as a parameter. Observe that $\lambda n=\mathcal{N}_D/V_{\mathrm{tot}}$ is the number of droplets per unit volume.

The Coulomb shift in a nanoscale defect was estimated as[11]

$$\varphi = \frac{Ze^2\Delta\kappa}{\epsilon r_D}, \tag{A2}$$

where e is the electron charge, the RE ion is taken as a donor with an effective uncompensated positive charge $Z|e|$, and ϵ is the dielectric constant. The ESR and dc magnetization data show that RE enters as RE^{3+} in the a-Si matrix.[15] Two (s-d) electrons form saturated bonds with (s-p) electrons of the neighboring Si, while the third (s-d) electron remains itinerant; thus at nanoscale distances, each RE ion acts as an effective one-electron donor in the a-Si host. For a-Gd_xSi_{1-x}, $Z\approx1$, $\epsilon\approx12-15$, the width of the itinerant electron band is $W\approx6-8$ eV, the average volume of the elementary cell is $a^3\approx20$ Å^3, i.e., the average lattice spacing is $a\approx2.7$ Å. For the nominal chemical composition $x=0.14$, the average concentration of RE ions is $n_{\mathrm{Gd}}=x/a^3\approx7\times10^{21}$ cm^{-3},[4,5] and we can estimate $\Delta\kappa\approx5-15$, $\lambda\approx0.01-0.03$ from the results of Refs. 10–14.

APPENDIX B: SHORT-RANGE FERROMAGNETIC ORDER

We recall here the description of both the paramagnetic phase and the phase with short-range ferromagnetic order.[11] We take $W/2$ as the unit energy and a as the unit length, and attach the subscript p, labeling the paramagnetic phase, to all quantities that have a different value in the two phases. The local DOS is $\varrho(\varepsilon)=\pi^{-1}\,\mathrm{Im}\langle G_A(\mathbf{r},\mathbf{r};\varepsilon)\rangle$, where ε is the electron energy and $\langle G_A(\mathbf{r},\mathbf{r};\varepsilon)\rangle$ is the advanced one-particle Green's function associated with the Hamiltonian (A1), averaged over the realizations of the disorder. In the absence of magnetic order, $\langle\vec{S}_i\rangle=0$ and $\varrho(\varepsilon)=\pi^{-1}\,\mathrm{Im}\int_{-\infty}^{+\infty}\varrho_0(z)[\varepsilon-z-\Sigma_A(\varepsilon)]^{-1}dz$, where the energy ε is measured from the center of the ideal lattice band and $\varrho_0(z)$ is the DOS of the ideal lattice spectrum $E(\mathbf{k})$. For the sake of definiteness we adopt a semielliptic form $\varrho_0(z)=2\pi^{-1}\sqrt{1-z^2}$, for $|z|\leqslant1$, and $\varrho_0(z)=0$, for $|z|>1$. This assumption is particularly reasonable when the number of doped carriers in the conduction band is not too large and the effective-mass approximation is valid.

The advanced self-energy $\Sigma_A(\varepsilon)$ is obtained by averaging over the realizations of the disorder within some scheme (e.g., the coherent potential approximation[16]). As customary, $\langle U(\mathbf{r})\rangle$ is included in the chemical potential μ. For uncorrelated impurities, the noncrossing Born approximation yields $\langle[U(\mathbf{r})]^2\rangle=[\mathcal{V}^2+S(S+1)\mathcal{J}^2]n_{\mathrm{imp}}$, where n_{imp} is the impurity

concentration. Explicit results for $\Sigma_A(\varepsilon)$ were obtained for different values of the parameter $b=\langle[2U/W]^2\rangle$.[7,8] We assume for simplicity a homogeneous broadening of the DOS, with an inverse lifetime $2\Gamma \propto b$, and take $\Sigma_A(\varepsilon)=i\Gamma$. Although this assumption seems very crude, and would be inadequate in the low-temperature regime where the metal-insulator transition occurs, it becomes fairly reasonable when describing the magnetic transformations occurring at higher temperatures. Indeed, we point out that the droplets are characterized by a large DOS at the Fermi level (see below), so that the description of short-range ferromagnetic order in the droplets should not be significantly affected by neglecting the frequency dependence of $\Sigma_A(\varepsilon)$. Then

$$\varrho(\varepsilon)=\frac{2}{\pi}\left\{\sqrt{\frac{1}{2}[\sqrt{(\varepsilon^2-\Gamma^2-1)^2+4\Gamma^2\varepsilon^2}-\varepsilon^2+\Gamma^2+1]}-\Gamma\right\}, \tag{B1}$$

which obviously yields ϱ_0 when $\Gamma \to 0$.

We treated the exchange part of the Hamiltonian (A1) in the mean-field approximation, taking $\langle \vec{S}_i \rangle = 0$ in the matrix and $\langle \vec{S}_i \rangle \neq 0$ inside the droplets. This is reasonable over a wide temperature range, since the local DOS at the Fermi level is larger in the droplets than in the matrix (see below), so that the condition for ferromagnetic ordering in the presence of an exchange coupling between magnetic RE ions and electrons is more easily realized in the droplets. The magnetic RE ions inside a nanoscale defect experience an effective magnetic field $H_{\text{eff}}=\mathcal{J}\int_{-\infty}^{+\infty}\Sigma_{\sigma=\pm1}\sigma\varrho_D(\varepsilon+\sigma m)\mathcal{F}(\varepsilon-\mu-\varphi)d\varepsilon$, where $\mathcal{F}(z)=[\exp(z/T)+1]^{-1}$ is the Fermi function at a temperature T (here we take $k_B=1$ and $\hbar=1$), $m \equiv \mathcal{J}x_D\langle S_z\rangle$ is the exchange-band splitting, $x_D=\gamma x$ is the concentration of magnetic RE ions per unit cell in a nanoscale defect, the index z defines the local quantization axis, parallel to the effective field, and the average value of the spin on the RE site, $\langle S_z\rangle$, is defined self-consistently as $\langle S_z\rangle = S\mathcal{B}_S(SH_{\text{eff}}/T)$, where $\mathcal{B}_S(y)=\mathcal{X}_S\coth(\mathcal{X}_S y)-\mathcal{Y}_S\coth(\mathcal{Y}_S y)$ is the Brillouin function for a spin S, with $\mathcal{X}_S=(2S+1)/(2S)$ and $\mathcal{Y}_S=1/(2S)$. The typical value of the exchange potential (in units of $W/2$) is $|\mathcal{J}|S\approx 0.1-0.2 \ll \varphi$ (see below).

The self-consistency equations must be solved together with the equations for μ and κ, which enforce global particle conservation and charge neutrality for an isolated droplet,

$$x=f\int_{-\infty}^{+\infty}\sum_{\sigma=\pm1}\varrho_D(\varepsilon+\sigma m)\mathcal{F}(\varepsilon-\mu-\varphi)d\varepsilon + 2(1-f)\int_{-\infty}^{+\infty}\varrho_M(\varepsilon)\mathcal{F}(\varepsilon-\mu)d\varepsilon,$$

$$x=\gamma^{-1}\int_{-\infty}^{+\infty}\sum_{\sigma=\pm1}\varrho_D(\varepsilon+\sigma m)\mathcal{F}(\varepsilon-\mu-\varphi)d\varepsilon.$$

Here, the factor 2 accounts for spin degeneracy in the matrix, and $x=na^3$. We assume for simplicity that Γ is the same in the matrix and in the droplets, i.e., $\varrho_M(\varepsilon)=\varrho_D(\varepsilon)$. However, this assumption is only aimed at reducing the number of parameters, and we could not only take $\Gamma_D \neq \Gamma_M$, but even adopt a different functional expression for the DOS in the matrix and in the droplets.

The chemical potential is the same in the two phases $\mu(T)=\mu_p(T)$.[11] In the paramagnetic phase $\langle \vec{S}_i \rangle = 0$, $m=0$. The self-consistency equations were numerically solved for typical parameters, $x=0.14$, $W=8$ eV, $\epsilon=12$, $\Delta\kappa=9$, $\lambda\approx 0.029$, and $\Gamma\approx 0.1$. This yielded, e.g., at $T=0$, $\mu_p=-1.0$, $\kappa_p\approx 3.1$, and hence $f_p\approx 0.091$, $\gamma_p\approx 3.34$, $\kappa_{D,p}\approx 10.4$, $v_{D,p}\approx 440$ Å^3, $r_{D,p}\approx 4.7$ Å. The Coulomb shift is $\varphi_p\approx 0.51$ (≈ 2 eV). The local DOS at the Fermi level are $\varrho_M(\mu_p)\approx 0.14$ and $\varrho_D(\mu_p+\varphi_p)\approx 0.50$, the maximum value being $\varrho_{\max}\approx 0.58$ for the chosen set of parameters. Hence, $A \equiv \varrho_D(\mu_p+\varphi_p)/\varrho_M(\mu_p) \approx 3.6$. These values are indicative and can be varied by changing the model parameters.

Our results for the paramagnetic phase are valid for both a-Gd_xSi_{1-x} [at temperatures larger than the temperature for the onset of ferromagnetic order in the droplets, defined below, Eq. (B2)] and a-Y_xSi_{1-x}. For small f_p the electron states within the droplets are localized and separated from the matrix by the surface-energy barrier and also the electron states within the tail of the matrix DOS are localized on the scale of interatomic distances. Therefore, the fraction of itinerant electrons within the elementary cell can be estimated as $x_{itin,p}=2(1-f_p)\int_{\varepsilon_m}^{+\infty}\varrho_M(\varepsilon)\mathcal{F}(\varepsilon-\mu_p)d\varepsilon$, where ε_m is the mobility edge, which depends on the scattering potential. For simplicity, we assumed that it lays at the bottom of the ideal band, so that the localized states are those that appear as tails of the disorder-broadened DOS [Eq. (B1)]. In any case, itinerant electrons are a tiny fraction of all the electrons in the conduction band, the greatest part being localized: for a nominal density of doped conduction electrons $n\approx 7\times 10^{21}$ cm^{-3}, the calculated density of itinerant electrons is $n_{itin,p}\approx 4\times 10^{19}$ cm^{-3} even at $T\approx 200$K. In Ref. 11 it was shown that $x_{itin,p}$ increases almost linearly with increasing T, consistently with the experiments (see Fig. 4).

We also studied the phase with short-range ferromagnetic order, assuming m as a small expansion parameter, and looking for solutions of the self-consistency equations close to the paramagnetic phase. The characteristic temperature for the onset of ferromagnetic order inside the droplets was thereby obtained as

$$T_D=\frac{2a^3}{3v_D}\mathcal{J}^2S(S+1)\kappa_D\varrho_D(\mu_p+\varphi_p). \tag{B2}$$

For the set of parameters suitable to a-$Gd_{0.14}Si_{0.86}$, and taking $|\mathcal{J}|\approx 0.026$ (≈ 0.1 eV, a typical exchange energy in wide-band magnetic semiconductors) we obtained, e.g., $T_D=0.0016$ (≈ 70K).

[1] F. Hellman, M. Q. Tran, A. E. Gebala, E. M. Wilcox, and R. C. Dynes, Phys. Rev. Lett. **77**, 4652 (1996).
[2] B. L. Zink, E. Janod, K. Allen, and F. Hellman, Phys. Rev. Lett. **83**, 2266 (1999).
[3] F. Hellman, D. R. Queen, R. M. Potok, and B. L. Zink, Phys. Rev. Lett. **84**, 5411 (2000).
[4] B. L. Zink, V. Preisler, D. R. Queen, and F. Hellman, Phys. Rev. B **66**, 195208 (2002).
[5] L. Bokacheva, W. Teizer, F. Hellman, and R. C. Dynes, Phys. Rev. B **69**, 235111 (2004).
[6] E. Helgren, J. J. Cherry, L. Zeng, and F. Hellman, Phys. Rev. B **71**, 113203 (2005).
[7] S. Kumar and P. Majumdar, Int. J. Mod. Phys. B **15**, 2683 (2001).
[8] P. Majumdar and S. Kumar, Phys. Rev. Lett. **90**, 237202 (2003).
[9] I. M. Lifshitz, S. A. Gradescul, and L. A. Pastur, *Introduction to the Theory of Disordered Systems* (Nauka, Moscow, 1982).
[10] N. K. Chumakov, S. V. Gudenko, V. V. Tugushev, A. B. Davydov, V. I. Ozhogin, E. Helgren, and F. Hellman, J. Magn. Magn. Mater. **272–276**, 1351 (2004).
[11] S. Caprara and V. V. Tugushev, Microelectron. Eng. **81**, 293 (2005).
[12] N. K. Chumakov, V. V. Tugushev, S. V. Gudenko, O. A. Nikolaeva, V. N. Lazukov, I. N. Goncharenko, and P. A. Alekseev, JETP Lett. **81**, 292 (2005).
[13] S. V. Gudenko, JETP Lett. **81**, 400 (2005).
[14] S. Caprara, V. V. Tugushev, and N. K. Chumakov, J. Exp. Theor. Phys. **101**, 305 (2005).
[15] M. Sercheli, C. Rettori, and A. Zanatta, Braz. J. Phys. **2**, 409 (2002).
[16] F. Yonezawa and K. Morigaki, Suppl. Prog. Theor. Phys. **53**, 1 (1973).
[17] W. Teizer, F. Hellman, and R. C. Dynes, Phys. Rev. Lett. **85**, 848 (2000).
[18] K. Yosida, Phys. Rev. **106**, 893 (1957).
[19] S. E. Barnes, Adv. Phys. **30**, 801 (1981).
[20] A. Abragam, *The Principles of Nuclear Magnetism* (Clarendon, Oxford, 1961).
[21] A. Abragam and B. Bleaney, *Electron Paramagnetic Resonance of Transition Ions* (Clarendon, Oxford, 1970).
[22] D. L. Huber, G. Alejandro, A. Caneiro, M. T. Causa, F. Prado, M. Tovar, and S. B. Oseroff, Phys. Rev. B **60**, 12155 (1999).
[23] S. A. Al'tshuler and B. M. Kozyrev, *Electron Paramagnetic Resonance* (Fizmatgiz, Moscow, 1961/Academic, New York, 1964).
[24] R. J. Elliott, Phys. Rev. **96**, 266 (1954).
[25] S. A. Al'tshuler and B. M. Kozyrev, *Electron Paramagnetic Resonance in Compounds of Transition Elements*, 2nd ed. (Nauka, Moscow, 1972/Halsted, New York, 1975).
[26] D. R. Hutton and G. J. Troup, Br. J. Appl. Phys. **15**, 405 (1964).
[27] I. Svare and G. Seidel, Phys. Rev. **134**, A172 (1964).
[28] D. Haskel, J. W. Freeland, J. Cross, R. Winarski, M. Newville, and F. Hellman, Phys. Rev. B **67**, 115207 (2003).
[29] E. M. Lifshitz and L. P. Pitaevsky, *Statistical Physics. Theory of Condensed Matter*, Theoretical Physics, Vol. 9, Part 2 (Fizmatgiz, Moscow, 2002).